

Tet3 regulates synaptic transmission and homeostatic plasticity via DNA oxidation and repair

Huimei Yu^{1,2}, Yijing Su^{1,2}, Jaehoon Shin^{1,7}, Chun Zhong^{1,2}, Junjie U Guo^{1,2,10}, Yi-Lan Weng^{1,2}, Fuying Gao³⁻⁶, Daniel H Geschwind³⁻⁶, Giovanni Coppola³⁻⁶, Guo-li Ming^{1,2,7-9} & Hongjun Song^{1,2,7,8}

Contrary to the long-held belief that DNA methylation of terminally differentiated cells is permanent and essentially immutable, post-mitotic neurons exhibit extensive DNA demethylation. The cellular function of active DNA demethylation in neurons, however, remains largely unknown. Tet family proteins oxidize 5-methylcytosine to initiate active DNA demethylation through the base-excision repair (BER) pathway. We found that synaptic activity bi-directionally regulates neuronal Tet3 expression. Functionally, knockdown of Tet or inhibition of BER in hippocampal neurons elevated excitatory glutamatergic synaptic transmission, whereas overexpressing Tet3 or Tet1 catalytic domain decreased it. Furthermore, dysregulation of Tet3 signaling prevented homeostatic synaptic plasticity. Mechanistically, Tet3 dictated neuronal surface GluR1 levels. RNA-seq analyses further revealed a pivotal role of Tet3 in regulating gene expression in response to global synaptic activity changes. Thus, Tet3 serves as a synaptic activity sensor to epigenetically regulate fundamental properties and meta-plasticity of neurons via active DNA demethylation.

Emerging evidence supports critical roles of epigenetic modifications, including both histone and DNA modifications, in neuronal plasticity, learning and memory, and in neurological and psychiatric disorders¹⁻⁵. Cytosine methylation is the predominant covalent modification of eukaryotic genomic DNA and regulates transcription in a highly cell type- and genomic context-dependent manner^{6,7}. The notion that methylation of cytosine in the genomic DNA of terminally differentiated cells is largely irreversible has been overturned by demonstrations of the loss of cytosine methylation in non-proliferating cells, such as post-mitotic neurons⁸⁻¹⁶. In particular, genome-wide studies with the single-base resolution in neurons have revealed large-scale changes in DNA methylation status during development and in response to neuronal activity^{14,15,17}, suggesting that dynamic DNA methylation could make a functional contribution to these biological processes^{2,4,5}.

The functional role of neuronal DNA demethylation, however, is not well understood, as we have limited knowledge of its underlying molecular mechanisms. One breakthrough came from the identification of Ten-eleven translocation (Tet) family proteins (Tet1-3), which oxidize 5-methylcytosine (5mC) into 5-hydroxymethylcytosine (5hmC) to initiate the active DNA demethylation process^{18,19}. Subsequent studies have shown that Tet-initiated active DNA demethylation is mediated through the base-excision DNA repair pathway in

neurons¹³ and in various other cell types^{20,21}. The mammalian brain contains the highest 5hmC levels^{22,23}, which are dynamically regulated under physiological and pathological conditions^{23,24}. Advances in our understanding of the molecular machinery mediating active DNA demethylation provide essential tools and an entry point to start to address the causal role of this pathway in neurons. Recent studies have revealed critical roles of Tet family members in activity-regulated neuronal gene expression¹³, as well as memory formation and extinction²⁵⁻²⁷. Because Tet proteins are known to exhibit functions independent of DNA demethylation activity^{28,29}, it remains unclear whether DNA demethylation is directly required in these functions. In addition, cellular processes regulated by active DNA demethylation in neurons are completely unknown. Given that active DNA demethylation requires oxidation and subsequent excision repair of genomic DNA, the question remains as to whether and how a pathway that effectively culminates in an insult to the genome and potential disruption of genomic stability could be critical for recurrent cellular processes in post-mitotic neurons that exist for decades or a lifetime.

We investigated cellular functions of the Tet-mediated active DNA demethylation pathway in hippocampal neurons. We found that synaptic activity bi-directionally regulated neuronal Tet3 expression, which in turn affected excitatory glutamatergic synaptic transmission via modulation of surface GluR1 levels. Furthermore, dysregulation of

¹Institute for Cell Engineering, Johns Hopkins University School of Medicine, Baltimore, Maryland, USA. ²Department of Neurology, Johns Hopkins University School of Medicine, Baltimore, Maryland, USA. ³Semel Institute for Neuroscience and Human Behavior, David Geffen School of Medicine, University of California Los Angeles, Los Angeles, California, USA. ⁴Program in Neurogenetics, David Geffen School of Medicine, University of California Los Angeles, Los Angeles, California, USA. ⁵Department of Neurology, David Geffen School of Medicine, University of California Los Angeles, Los Angeles, California, USA. ⁶Department of Psychiatry, David Geffen School of Medicine, University of California Los Angeles, Los Angeles, California, USA. ⁷Graduate Program in Cellular and Molecular Medicine, Johns Hopkins University School of Medicine, Baltimore, Maryland, USA. ⁸The Solomon H. Snyder Department of Neuroscience, Johns Hopkins University School of Medicine, Baltimore, Maryland, USA. ⁹Department of Psychiatry and Behavioral Sciences, Johns Hopkins University School of Medicine, Baltimore, Maryland, USA. ¹⁰Present address: Whitehead Institute for Biomedical Research, Cambridge, Massachusetts, USA. Correspondence should be addressed to H.S. (shongju1@jhmi.edu).

Received 8 February; accepted 25 March; published online 27 April 2015; doi:10.1038/nn.4008

Tet3-mediated DNA demethylation signaling prevented homeostatic synaptic plasticity. RNA-seq analyses also showed a pivotal role of Tet3 in regulating gene expression in response to global synaptic-activity changes. These results reveal a functional role of active DNA demethylation signaling as a synaptic activity sensor that regulates fundamental properties of neurons.

RESULTS

Activity-dependent expression of Tet3 regulates synaptic transmission

To identify the potential role of Tet proteins in neuronal function, we first characterized the expression of Tet family members in hippocampal neurons under basal conditions and following changes of neuronal circuit activity. Quantitative PCR analysis revealed that mRNA levels of Tet3, but not Tet1 and Tet2, were substantially increased after global synaptic activity was elevated in the presence of bicuculline (20 μ M) and decreased when global synaptic activity was reduced in the presence of tetrodotoxin (TTX; 1 μ M; **Fig. 1a** and **Supplementary Table 1a**). We confirmed Tet3 protein level changes at 4 h after different treatments (**Fig. 1b**). These results establish that neuronal Tet3 expression is bi-directionally regulated by changes in global synaptic activity.

Tet3 protein is localized in the nucleus of neurons (**Supplementary Fig. 1a**). To examine the effect of Tet3 expression in neurons, we used AAV to coexpress EYFP and shRNAs specific to mouse Tet3 in cultured hippocampal neurons (**Supplementary Fig. 1b** and **Supplementary Table 1b**). shRNA-Tet3-1 and shRNA-Tet3-2 (ref. 19), but not a control shRNA (sh-control), effectively reduced endogenous Tet3 expression in neurons at both the mRNA and protein levels without any changes in Tet1 and Tet2 mRNA expression (**Fig. 1b** and **Supplementary Fig. 1c**). Dot-blot analyses showed no

differences in global 5hmC levels in neurons with Tet3 knockdown (Tet3-KD; **Supplementary Fig. 1d**), likely as a result of the presence of Tet1 and Tet2 in these neurons. Whole-cell patch-clamp recording of EYFP⁺ neurons also revealed no substantial differences in firing properties (**Supplementary Fig. 1e**). Immunocytochemistry analyses showed similar densities of synapsin I⁺ synaptic boutons under different conditions (**Supplementary Fig. 1f**). Thus, Tet3 deficiency did not appear to generally affect global neuronal properties. Notably, electrophysiological recordings revealed that Tet3-KD neurons, using two independent shRNAs, exhibited substantially larger miniature glutamatergic excitatory postsynaptic current (mEPSC) amplitudes than neurons expressing sh-control (**Fig. 1c**). Conversely, neurons transfected with a construct coexpressing EYFP and Tet3 (Tet3 OE) exhibited significantly smaller mEPSC amplitudes than neurons expressing EYFP alone ($P = 0.002$; **Fig. 1d**). Given that less than 5% of neurons were transfected in these experiments, the effect of Tet3 overexpression is likely to be cell autonomous. Together, our results indicate that neuronal Tet3 levels bi-directionally affect excitatory synaptic transmission.

Tet3 regulates synaptic transmission via DNA oxidation and repair

Given that hippocampal neurons express Tet1 and Tet2 at constant levels, we also examined the effect of Tet1 or Tet2 knockdown on synaptic transmission. We developed efficient shRNAs specific to Tet1 and Tet2, and AAV-mediated expression of the shRNAs reduced Tet1 or Tet2 levels in neurons, respectively (**Supplementary Fig. 1c**). Notably, neurons with decreased expression of either Tet1 or Tet2 also exhibited increased mEPSC amplitudes compared with those expressing sh-control, although the effect was modest in comparison

Figure 1 Synaptic activity-dependent expression of Tet3 regulates glutamatergic synaptic transmission. **(a)** Expression of Tet family members in response to changes of global synaptic activity. Shown are summaries of time-course analysis of mRNA expression of Tet1–3 in cultured mouse hippocampal neurons after continuous presence of TTX (1 μ M) or bicuculline (Bicu, 20 μ M). The same cultures were used for analysis of expression of three Tet genes and data was normalized to time zero for parallel cultures. Values represent mean \pm s.e.m. ($n = 3$ cultures; $*P < 0.05$, ANOVA; for Tet3 plot of TTX treatment, $P = 0.5$ at 0 h, $P = 0.00007$ at 1 h, $P = 0.003$ at 4 h, $P = 0.002$ at 12 h, $P = 0.03$ at 24 h and $P = 0.07$ at 48 h; for Tet2 bicuculline treatment: $P = 0.5$ at 0 h, $P = 0.02$ at 1 h, $P = 0.01$ at 4 h, $P = 0.006$ at 12 h, $P = 0.02$ at 24 h and $P = 0.50$ at 48 h). **(b)** Western blot analysis of neuronal Tet3 protein levels following different treatments. Hippocampal neurons in culture were treated with saline, TTX (1 μ M) or bicuculline (20 μ M) for 4 h, or infected with AAV to express control shRNA (sh-control) or two different shRNAs specific for mouse Tet3 (sh-Tet3-1, sh-Tet3-2). Shown are cropped sample western blot images (left; full-length blots are presented in **Supplementary Fig. 11**) and quantification of Tet3 protein levels (right). Values represent mean \pm s.e.m. ($n = 3$; $***P < 0.001$, $**P < 0.01$, $*P < 0.05$, ANOVA; $P = 0.006$, vehicle versus TTX; $P = 0.02$, vehicle versus bicuculline; $P = 0.0002$, sh-control versus sh-Tet3-2; $P = 0.0003$, sh-control versus sh-Tet3-1). **(c)** Tet3-KD neurons exhibited elevated glutamatergic synaptic transmission. Shown are sample whole-cell voltage-clamp recording traces of hippocampal neurons coexpressing EYFP and different shRNAs (left) and cumulative distribution plot of mEPSC amplitudes (right). Inset, summary of mean mEPSC amplitudes. The numbers in the bar graphs indicate the numbers of neurons examined. Values represent mean \pm s.e.m. ($***P < 0.001$, $**P < 0.01$, Kolmogorov-Smirnov test; $P = 0.003$, sh-control versus sh-Tet3-1; $P = 0.00009$, sh-control versus sh-Tet3-2). **(d)** Neurons overexpressing Tet3 exhibited decreased glutamatergic synaptic transmission. Data are presented as in **c**, except that neurons were transfected with vectors to express EYFP or coexpress EYFP and Tet3 (Tet3 OE). Values represent mean \pm s.e.m. ($**P < 0.01$, Kolmogorov-Smirnov test; $P = 0.002$, EYFP versus Tet3 OE).

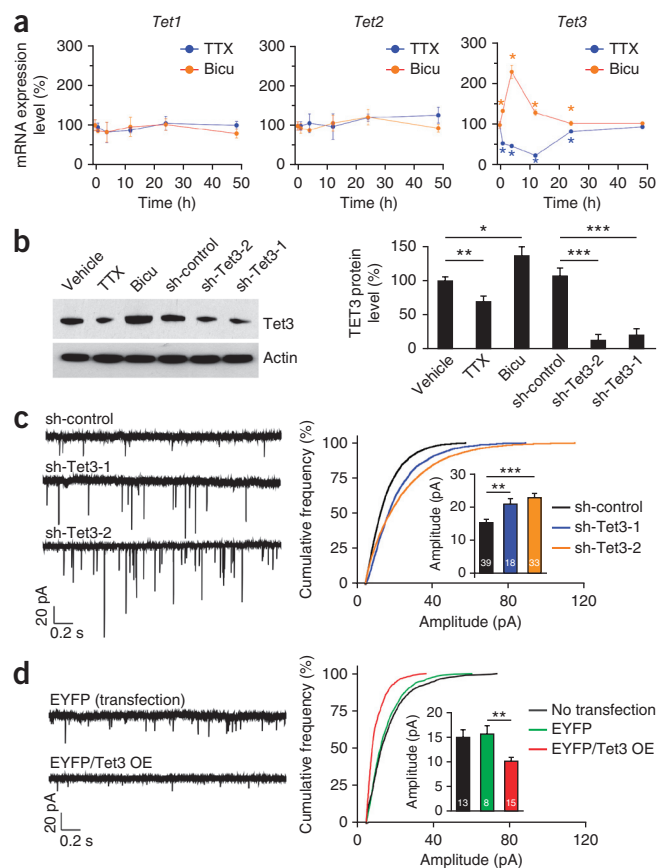
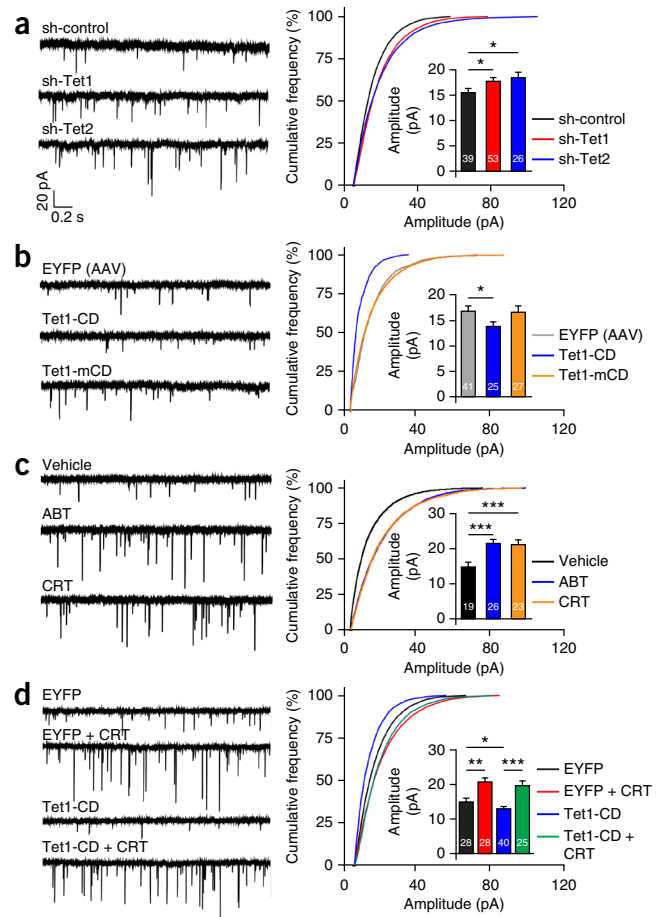


Figure 2 DNA oxidation and BER regulates glutamatergic synaptic transmission. (a,b) Data are presented as in **Figure 1c,d**, except that neurons were infected with AAV to coexpress EYFP and shRNA specific to Tet1 or Tet2 (a), Tet1-CD or its enzymatic dead mutant (Tet1-mCD) (b), or treated with vehicle, ABT (50 μ M), or CRT (50 μ M), for 48 h before analysis of wild-type neurons (c) or neurons expressing Tet1-CD (d). Values represent mean \pm s.e.m. (** $P < 0.001$, * $P < 0.05$, Kolmogorov-Smirnov test; a, $P = 0.02$, sh-control versus sh-Tet1 and $P = 0.01$, sh-control versus sh-Tet2; b, $P = 0.01$, EYFP versus Tet1-CD; c, $P = 0.00005$, vehicle versus ABT and $P = 0.0005$, vehicle versus CRT; d, $P = 0.002$, EYFP versus EYFP + CRT; $P = 0.02$, EYFP versus Tet1-CD; $P = 0.00005$, Tet1-CD versus Tet1-CD + CRT).

with Tet3-KD (**Fig. 2a**). In addition, AAV-mediated overexpression of the catalytic domain of Tet1 (Tet1-CD), but not a dioxygenase-dead mutant¹³ (Tet1-mCD), decreased mEPSC amplitudes (**Fig. 2b**), which was accompanied by increased total 5hmC levels (**Supplementary Fig. 1d**). Thus, changes in DNA oxidation activity in neurons are sufficient to modulate basal levels of synaptic transmission.

Tet proteins are known to exhibit oxidation-independent functions in embryonic stem cells^{28,29} and in neurons²⁵. On the other hand, Tet-induced active, region-specific DNA demethylation is mediated by the BER pathway^{13,30,31}. To further investigate the molecular mechanism by which Tet regulates synaptic transmission, we used two inhibitors of critical BER components, poly(ADP-ribose) polymerase inhibitor ABT-888 (ABT) and apurinic/aprimidinic endonuclease inhibitor CRT0044876 (CRT), which have been shown to block DNA demethylation in mouse zygotes³² and Tet1-CD-induced DNA demethylation in mammalian cells¹³. Treatment with ABT (50 μ M) or CRT (50 μ M) for 48 h led to increased mEPSC amplitudes (**Fig. 2c**), resembling the Tet KD effect. Furthermore, the reduced mEPSC amplitude from Tet1-CD overexpression was normalized to the same level as that of control neurons following CRT treatment, suggesting that BER functions downstream of DNA oxidation to regulate synaptic transmission (**Fig. 2d**). Together, these results suggest that Tet regulates basal levels of excitatory synaptic transmission in neurons through DNA oxidation and subsequent BER.



Tet3 is required for homeostatic synaptic plasticity

Given that Tet3 expression was bi-directionally regulated by TTX and bicuculline treatments (**Fig. 1a**), which are well-known to induce homeostatic synaptic scaling³³, we next focused on Tet3 and assessed whether it also regulates synaptic plasticity. Notably, both

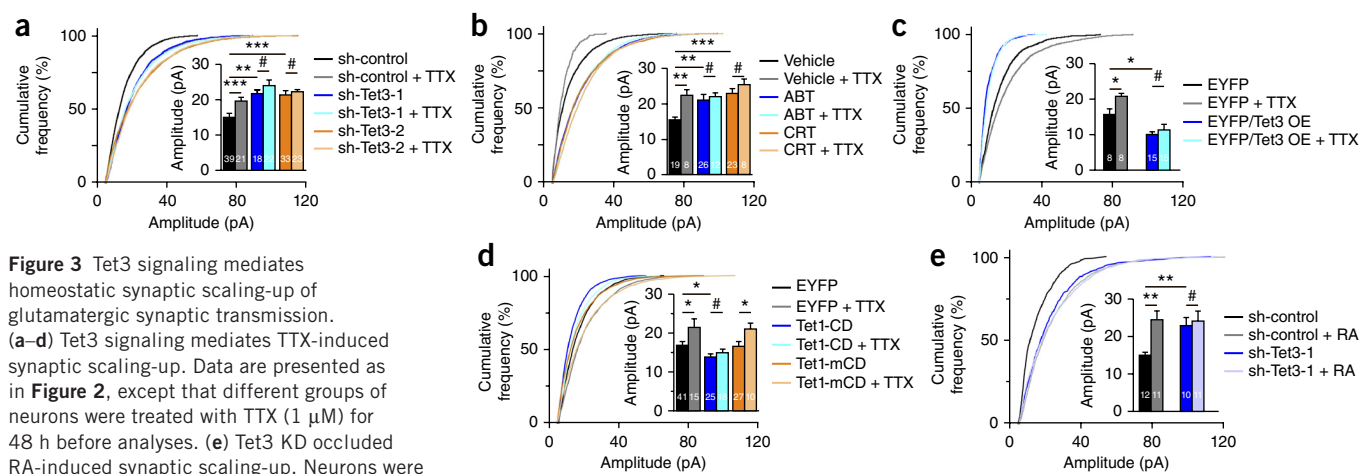


Figure 3 Tet3 signaling mediates homeostatic synaptic scaling-up of glutamatergic synaptic transmission. (a–d) Tet3 signaling mediates TTX-induced synaptic scaling-up. Data are presented as in **Figure 2**, except that different groups of neurons were treated with TTX (1 μ M) for 48 h before analyses. (e) Tet3 KD occluded RA-induced synaptic scaling-up. Neurons were infected with AAV to express different shRNAs and were treated with RA (1 μ M) for 2 h before analysis. (** $P < 0.001$, ** $P < 0.01$, * $P < 0.05$, # $P > 0.1$, Kolmogorov-Smirnov test; a, $P = 0.0003$, sh-control versus sh-control + TTX; $P = 0.30$, sh-Tet3-1 versus sh-Tet3-1 + TTX; $P = 0.12$, sh-Tet3-2 versus sh-Tet3-2 + TTX; $P = 0.003$, sh-control versus sh-Tet3-1; $P = 0.000009$, sh-control versus sh-Tet3-2; b, $P = 0.007$, vehicle versus vehicle + TTX; $P = 0.13$, ABT versus ABT + TTX; $P = 0.26$, CRT versus CRT + TTX; $P = 0.003$, vehicle versus ABT; $P = 0.0005$, vehicle versus CRT; c, $P = 0.014$ EYFP versus EYFP + TTX; $P = 0.24$, EYFP/Tet3 OE versus EYFP/Tet3 OE + TTX; $P = 0.01$ EYFP versus EYFP/Tet3 OE; d, $P = 0.04$, EYFP versus EYFP + TTX; $P = 0.19$, Tet1-CD versus Tet1-CD + TTX; $P = 0.02$, Tet1-mCD versus Tet1-mCD + TTX; $P = 0.01$, EYFP versus Tet1-CD; e, $P = 0.001$, sh-control versus sh-control + RA; $P = 0.37$, sh-Tet3-1 versus sh-Tet3-1 + RA; $P = 0.003$, sh-control versus sh-Tet3-1).

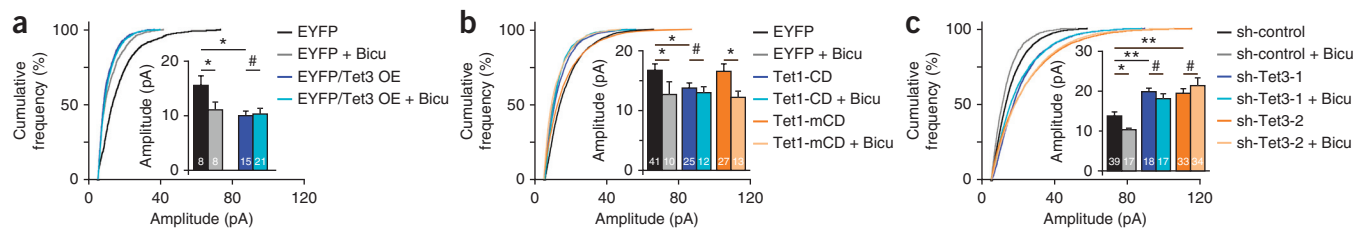


Figure 4 Tet3 signaling mediates bicuculline-induced homeostatic synaptic scaling-down of glutamatergic synaptic transmission. Data are presented as in **Figure 3a–d**, except that different groups of neurons were treated with bicuculline (20 μ M) for 48 h before analyses ($^{**}P < 0.01$, $^{*}P < 0.05$, $^{\#}P > 0.1$, Kolmogorov-Smirnov test; **a**, $P = 0.03$, EYFP versus EYFP + Bicu; $P = 0.42$, EYFP/Tet3 OE versus EYFP/Tet3 OE + Bicu; $P = 0.01$, EYFP versus EYFP/Tet3 OE; **b**, $P = 0.05$, EYFP versus EYFP + Bicu; $P = 0.28$, Tet1-CD versus Tet1-CD + Bicu; $P = 0.005$, Tet1-mCD versus Tet1-mCD + Bicu; $P = 0.01$, EYFP versus Tet1-CD; **c**, $P = 0.01$, sh-control versus sh-control + Bicu; $P = 0.15$, sh-Tet3-1 versus sh-Tet3-1 + Bicu; $P = 0.41$, sh-Tet3-2 versus sh-Tet3-2 + Bicu; $P = 0.00001$, sh-control versus sh-Tet3-2; **d**, $P = 0.003$, vehicle versus vehicle + Bicu; $P = 0.13$, ABT versus ABT + Bicu; $P = 0.20$, CRT versus CRT + Bicu; $P = 0.003$, vehicle versus ABT; $P = 0.0005$, vehicle versus CRT).

Tet3 KD and BER inhibition elevated mEPSC amplitudes linearly across the spectrum under basal conditions (**Supplementary Figs. 2a** and **3a**), which was comparable to the scaling-up effect induced by TTX treatment in normal neurons (**Supplementary Fig. 2c**). Thus, downregulation of Tet3 signaling appears to be sufficient to induce scaling-up. Furthermore, Tet3 KD and BER inhibition showed no additional scaling-up following TTX treatment (**Fig. 3a,b** and **Supplementary Figs. 2b** and **3b**), indicating occlusion of these two manipulations. On the other hand, overexpression of Tet3 or Tet1-CD, but not Tet1-mCD, completely prevented TTX-induced scaling-up (**Fig. 3c,d** and **Supplementary Figs. 4b,c** and **5b,c**), suggesting that downregulation of Tet signaling is required for scaling-up. Together, these results suggest that TTX treatment

downregulates Tet3 signaling, which mediates homeostatic scaling-up of excitatory synaptic transmission.

Homeostatic synaptic scaling-up of excitatory synaptic transmission has also been shown to be induced by all-trans retinoic acid (RA)³⁴. Although acute RA treatment (1 μ M) increased mEPSC amplitude in neurons expressing sh-control, there was no further amplitude increase in Tet3-KD neurons (**Fig. 3e** and **Supplementary Fig. 2f,g**), indicating that they also occlude each other. These results suggest that Tet3 signaling is required for different types of homeostatic synaptic plasticity.

Figure 5 Tet3 signaling regulates neuronal surface GluR1 levels. **(a)** Tet3 knockdown increased surface GluR1 levels and prevented further changes following TTX (1 μ M) or bicuculline (20 μ M) treatment for 48 h. Shown are sample confocal images of surface GluR1 immunostaining (left) and quantification (right). Signal intensity of each condition was normalized to that of neurons expressing sh-control vehicle treatment in parallel cultures. Values represent mean \pm s.e.m. ($n = 3$ cultures, $^{***}P < 0.001$, $^{*}P < 0.05$, $^{\#}P > 0.1$, ANOVA). Scale bar represents 10 μ m. **(b)** Expression of Tet1-CD, but not Tet1-mCD, decreased surface GluR1 levels and prevented further changes following TTX or bicuculline treatment. Data are presented as in **a**, except that neurons were infected with AAV to express EYFP, Tet1-CD or Tet1-mCD. Values represent mean \pm s.e.m. ($n = 3$ cultures, $^{***}P < 0.001$, $^{\#}P > 0.1$, ANOVA). Scale bar represents 10 μ m. **(c)** Western blot analyses of surface GluR1 levels under different conditions. Data are presented as in **a** and **b**, except that surface biotinylated GluR1 proteins were examined by western blot and quantified. Full-length blots are presented in **Supplementary Figure 11**. Values represent mean \pm s.e.m. ($n = 3$ cultures, $^{**}P < 0.01$, $^{*}P < 0.05$, $^{\#}P > 0.1$, ANOVA). **a**, $P = 0.000001$, sh-control versus sh-control + TTX; $P = 0.000001$, sh-control versus sh-control + Bicu; $P = 0.30$, sh-Tet3-1 versus sh-Tet3-1 + TTX; $P = 0.38$, sh-Tet3-1 versus sh-Tet3-1 + Bicu; $P = 0.20$, sh-Tet3-2 versus sh-Tet3-2 + TTX; $P = 0.42$, sh-Tet3-2 versus sh-Tet3-2 + Bicu; $P = 0.0000001$, sh-control versus sh-Tet3-1; $P = 0.0000001$, sh-control versus sh-Tet3-2; **b**, $P = 0.0000001$, EYFP versus EYFP + TTX; $P = 0.000001$, EYFP versus EYFP + Bicu; $P = 0.25$, Tet1-CD versus Tet1-CD + TTX; $P = 0.43$, Tet1-CD versus Tet1-CD + Bicu; $P = 0.0000001$, Tet1-mCD versus Tet1-mCD + TTX; $P = 0.0000001$, Tet1-mCD versus Tet1-mCD + Bicu; **c**, $P = 0.03$, sh-control versus sh-control + TTX; $P = 0.01$, sh-control versus sh-control + Bicu; $P = 0.38$, sh-Tet3-2 versus sh-Tet3-2 + TTX; $P = 0.09$, sh-Tet3-2 versus sh-Tet3-2 + Bicu; $P = 0.27$, Tet1-CD versus Tet1-CD + TTX; $P = 0.12$, Tet1-CD versus Tet1-CD + Bicu; $P = 0.004$, sh-control versus sh-Tet3-2; $P = 0.02$, sh-control versus Tet1-CD.

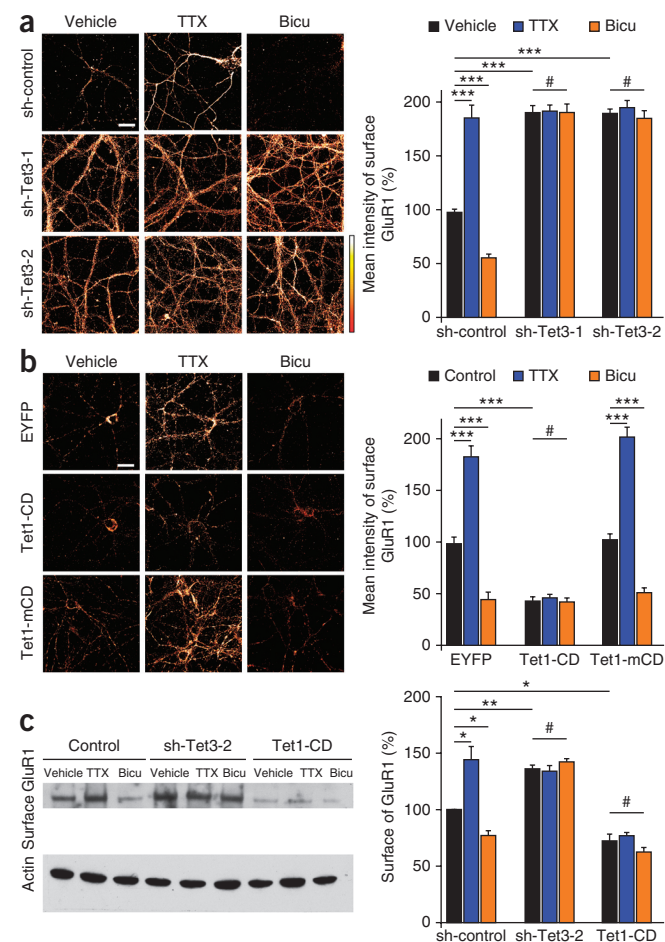
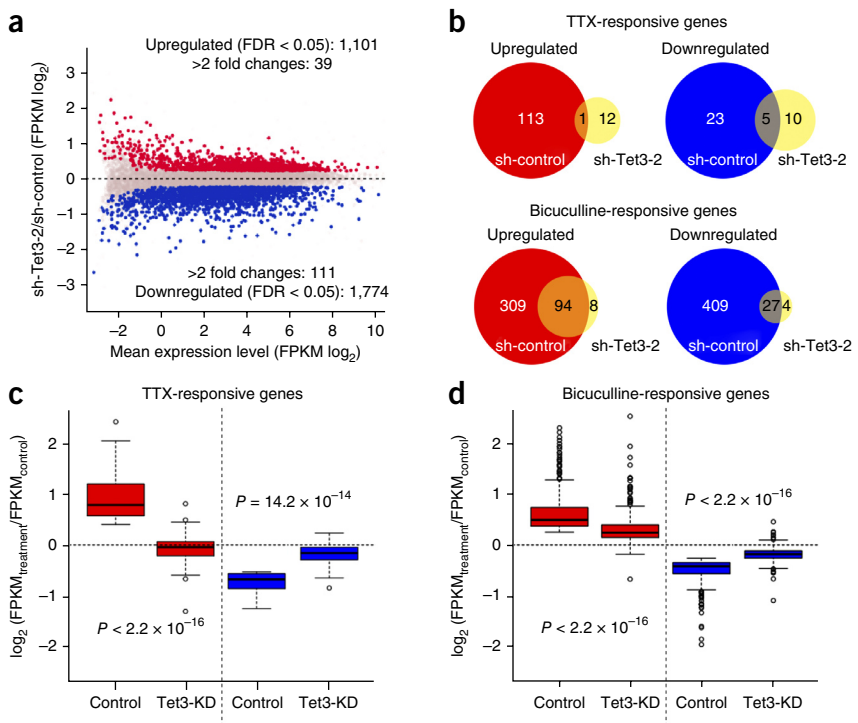


Figure 6 Tet3 regulates gene expression in neurons in response to global synaptic activity changes. **(a)** Comparison of gene expression in neurons expressing sh-control or sh-Tet3-2 by RNA-seq analyses. Shown is a summary dot plot, with red dots representing upregulated genes and blue dots representing downregulated genes ($n = 3$ samples each; $FDR < 0.05$). **(b)** Venn diagrams of differentially expressed genes at 4 h following TTX (1 μ M) or bicuculline (20 μ M) treatment in neurons expressing sh-control or sh-Tet3-2, as determined by RNA-seq analyses ($FDR < 0.05$). **(c,d)** Box-plot of mean expression levels of up- and downregulated genes in neurons expressing sh-control in response to TTX **(c)** or bicuculline **(d)** treatment and the expression of the same sets of genes in Tet3-KD neurons under the same condition (Wilcoxon rank-sum test; **c**, $P = 2.2 \times 10^{-16}$, upregulated genes; $P = 14.2 \times 10^{-14}$, down-regulated genes; **d**, $P < 2.2 \times 10^{-16}$, both upregulated and down-regulated genes). Center line: median value; box limits: 25th and 75th percentile values; whiskers: maximum and minimum data points excluding the outliers; outliers: data points that are higher or lower than the 1.5 times the quartile (25th and 75th) values.



Does bicuculline-induced Tet3 upregulation also regulate synaptic scaling-down? Indeed, neurons overexpressing Tet3 and Tet1-CD, but not Tet1-mCD, exhibited reduced mEPSC amplitudes linearly across the spectrum (**Supplementary Figs. 4a** and **5a**), resembling bicuculline-induced scaling-down in normal neurons (**Supplementary Fig. 4e**). Upregulating Tet3 signaling or oxidation activity via Tet1-CD also occluded bicuculline-induced scaling-down (**Fig. 4a,b** and **Supplementary Figs. 4d,e** and **5d,e**). In addition, downregulating Tet3 signaling via Tet3 KD or BER inhibition prevented bicuculline-induced scaling-down (**Fig. 4c,d** and **Supplementary Figs. 2d,e** and **3d,e**). These results suggest that global synaptic activity modulates Tet3 expression and DNA demethylation activity, which in turn mediate homeostatic synaptic scaling-up or scaling-down.

Tet3 regulates synaptic transmission and plasticity by modulating surface GluR1 levels

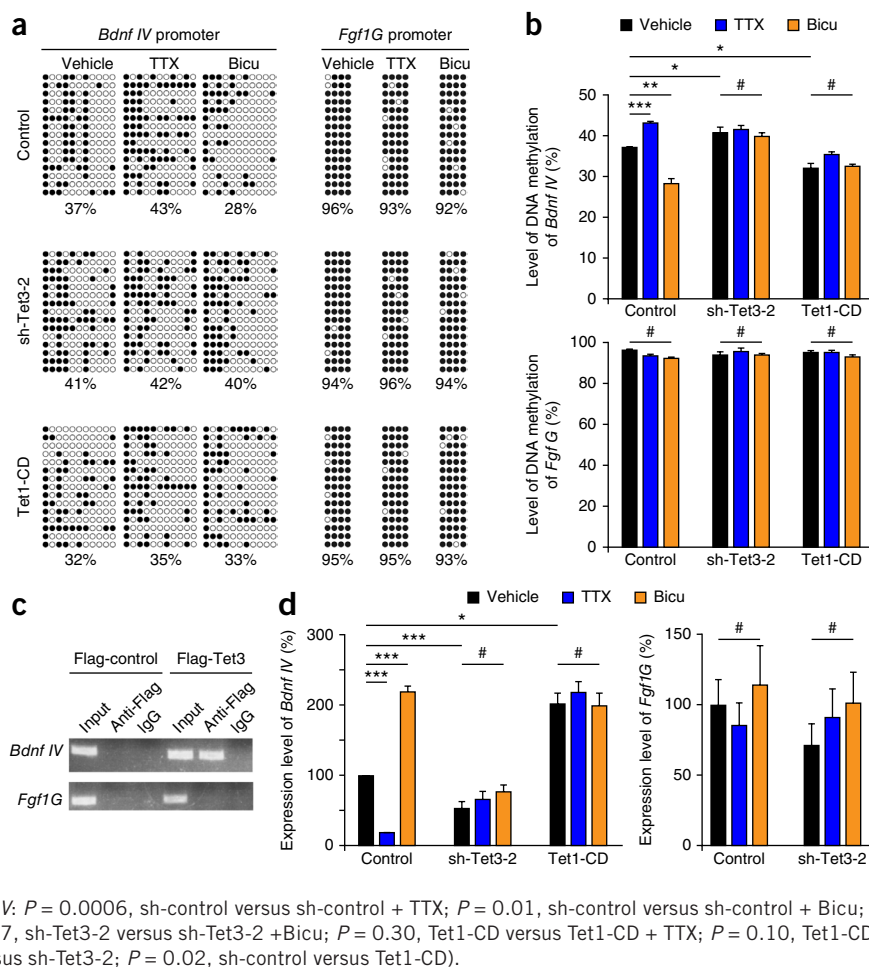
A key cellular mechanism regulating both basal glutamatergic synaptic transmission and homeostatic scaling is the control of surface levels of glutamate receptors³⁵. Using quantitative immunocytochemistry analysis, we found that Tet3-KD neurons exhibited elevated surface GluR1 levels; conversely, neurons overexpressing Tet1-CD, but not Tet1-mCD, displayed reduced levels of surface GluR1 (**Fig. 5a,b**). Quantitative western blot analyses also revealed bi-directional changes of surface GluR1 levels (**Fig. 5c**), but not total GluR1 levels (**Supplementary Fig. 6a**). There was no substantial change in either total or surface GluR2 levels following Tet3 KD or Tet1-CD expression (**Supplementary Fig. 7a**). Consistent with a change of functional GluR1 levels at synapses, treatment of NASPM (1-naphthyl acetyl spermine trihydrochloride), which blocks all GluR2-lacking AMPA receptors³⁶, led to a larger reduction of mEPSC amplitudes in Tet3-KD neurons than in neurons expressing sh-control (**Supplementary Fig. 7b**). Analysis of mEPSC decay time under different conditions was also consistent with changes in GluR1 levels at synapses (**Supplementary Fig. 7c**). Together, these results suggest that Tet3 regulates basal excitatory synaptic transmission via regulating surface GluR1 levels.

This same cellular mechanism also explains the role of Tet3 in homeostatic synaptic scaling. Tet3 KD was sufficient to elevate surface GluR1 levels and prevent further changes following TTX or bicuculline treatment (**Fig. 5a,c**). Conversely, overexpression of Tet1-CD was sufficient to reduce surface GluR1 levels and prevent further changes following bicuculline or TTX treatment (**Fig. 5b,c**). Thus, changes in Tet3 signaling are both sufficient and necessary for the TTX-induced increase and bicuculline-induced decrease in surface GluR1 expression and resultant synaptic scaling. The immediate early gene *Arc* is known to regulate GluR insertion and synaptic scaling^{37–39}. Notably, Tet3 KD led to decreased *Arc* protein levels, which mimics TTX-induced downregulation of *Arc*, and prevented bicuculline-induced *Arc* upregulation (**Supplementary Fig. 6b**). Thus, regulation of *Arc* levels appears to explain changes in surface GluR1 levels following Tet3 KD. Together, our results suggest that Tet3 and active DNA demethylation signaling respond to changes in global synaptic activity to re-establish a responsive cellular state.

Tet3 is essential for activity-induced gene expression changes and DNA demethylation

To further support this model and directly examine the role of Tet3 in synaptic activity-dependent gene expression, we performed RNA-seq analyses of sh-control and Tet3-KD neurons at 4 h after saline, TTX or bicuculline treatment (**Supplementary Fig. 8** and **Supplementary Table 2**). RNA-seq confirmed 70% knockdown efficacy for Tet3 mRNA levels in neurons expressing sh-Tet3-2 (**Supplementary Fig. 8a**). At the basal level, Tet3-KD neurons exhibited differential expression of a large number of genes compared with neurons expressing sh-control, with more genes downregulated than upregulated (**Fig. 6a** and **Supplementary Table 2b–g**). Notably, many genes related to synapses and synaptic transmission were differentially expressed (**Supplementary Fig. 9**). Multidimensional scaling, an unbiased method to quantify the degree of similarity between large data sets, showed clear segregation between sh-control and sh-Tet3-2 groups (**Supplementary Fig. 8c**). As expected, TTX or bicuculline treatments induced substantial

Figure 7 Essential role of Tet3 in neuronal activity-induced DNA methylation dynamics at the *Bdnf* IV promoter region and gene expression. **(a, b)** Bisulfite-sequencing analysis of control, Tet3-KD and Tet1-CD neurons at 4 h after treatment with saline, TTX or bicuculline. Sample bisulfite-sequencing results at the *Bdnf* promoter IV region and *Fgf1G* promoter regions are shown **(a)**. Each row represents one allele showing methylation status of individual CpG sites (open circle, unmethylated; closed circle, methylated). Mean values of methylate levels of all CpG sites for each region are also shown for each individual culture. A summary of results from multiple cultures is also shown **(b)**. A minimum of 15 alleles were examined for DNA methylation for each culture. Values represent mean \pm s.e.m. ($n = 3-6$ cultures, *** $P < 0.001$, ** $P < 0.01$, * $P < 0.05$, # $P > 0.1$, ANOVA; *Bdnf* IV, $P = 0.0006$, sh-control versus sh-control + TTX; $P = 0.007$, control versus control + Bicu; $P = 0.10$, sh-Tet3-2 versus sh-Tet3-2 + TTX; $P = 0.32$, sh-Tet3-2 versus sh-Tet3-2 + Bicu; $P = 0.30$, Tet1-CD versus Tet1-CD + TTX; $P = 0.37$, Tet1-CD versus Tet1-CD + Bicu; $P = 0.03$, control versus sh-Tet3-2; $P = 0.02$, control versus Tet1-CD). **(c)** ChIP-PCR analyses of Tet3 binding to *Bdnf* IV and *Fgf1G* promoter regions. Flag-tagged Tet3 was expressed in hippocampal neurons for analysis. Full-length blots are presented in **Supplementary Figure 11**. **(d)** Summary of mRNA expression under different conditions. Values represent mean \pm s.e.m. ($n = 3$ cultures, * $P < 0.05$, # $P > 0.1$, ANOVA; *Bdnf* IV: $P = 0.0006$, sh-control versus sh-control + TTX; $P = 0.01$, sh-control versus sh-control + Bicu; $P = 0.16$, sh-Tet3-2 versus sh-Tet3-2 + TTX; $P = 0.07$, sh-Tet3-2 versus sh-Tet3-2 + Bicu; $P = 0.30$, Tet1-CD versus Tet1-CD + TTX; $P = 0.10$, Tet1-CD versus Tet1-CD + Bicu; $P = 0.00004$, sh-control versus sh-Tet3-2; $P = 0.02$, sh-control versus Tet1-CD).



transcriptomic changes in neurons expressing sh-control, as shown by clear segregation among different groups (**Supplementary Fig. 8c**). In contrast, Tet3-KD neurons showed reduced segregation between saline and bicuculline treatment and no segregation between saline and TTX treatment (**Supplementary Fig. 8c**). Notably, of the TTX-responsive genes in control neurons (false discovery rate (FDR) < 0.05), 99% of upregulated and 85% of downregulated genes lost responsiveness in Tet3-KD neurons (**Fig. 6b**). Of the bicuculline-responsive genes in control neurons (FDR < 0.05), 77% of upregulated and 94% of downregulated genes lost responsiveness in Tet3-KD neurons, whereas very few genes were upregulated (8) or downregulated (4) specifically in Tet3-KD neurons (**Fig. 6b**). Further analysis of up- and downregulated genes in two separate populations showed that expression changes induced by TTX or bicuculline treatment were substantially attenuated in Tet3-KD neurons compared with in neurons expressing sh-control (**Fig. 6c,d**). Notably, bicuculline-induced expression of immediate early genes, including *Arc*, *c-Fos*, *Npas4* and *Egr4*, was largely unaffected in Tet3-KD neurons when examined at 4 h after treatment (**Supplementary Fig. 10a**), suggesting no general impairment of Tet3-KD neurons in response to neuronal activation. Taken together, these results identify an essential role of Tet3 in regulating gene expression in response to changes in global synaptic activity.

To ascertain that Tet3 can directly regulate gene expression via active DNA demethylation, we focused on *Bdnf*, the gene encoding brain-derived neurotrophic factor, which has been shown to exhibit active DNA demethylation in these neurons⁸ and has been implicated in regulating both excitatory synaptic transmission⁴⁰ and synaptic

scaling⁴¹. Bisulfite-sequencing analysis showed that Tet3-KD neurons exhibited increased CpG methylation at the *Bdnf* promoter IV region, whereas overexpressing Tet1-CD had the opposite effect (**Fig. 7a,b** and **Supplementary Table 1c**). Consistent with a lack of global changes in DNA methylation levels (**Supplementary Fig. 1d**), Tet3 KD did not affect CpG methylation at the *Fgf1G* promoter region (**Fig. 7a,b**) or the *Arc* and *Npas4* promoters (**Supplementary Fig. 10b**). Chromatin immunoprecipitation (ChIP)-PCR analysis further showed an association of Tet3 with the *Bdnf* IV region, but not the *Fgf1G* region, in neurons (**Fig. 7c** and **Supplementary Table 1d**). CpG methylation at the *Bdnf* IV region was substantially increased after TTX induced decreases in global synaptic activity and Tet3 expression (**Fig. 7a,b**). Conversely, bicuculline treatment increased Tet3 expression and decreased methylation at the same region (**Fig. 7a,b**). Accompanying methylation changes, neurons exhibited changes in *Bdnf* expression from the *Bdnf* IV promoter region, with increased gene expression resulting from decreased methylation (**Fig. 7d**). No changes in *Fgf1G* expression were detected under any conditions (**Fig. 7d**). Notably, neurons with Tet3 KD or Tet1-CD overexpression exhibited no further changes in either methylation levels or mRNA expression of *Bdnf* IV following TTX or bicuculline treatment (**Fig. 7a,b,d**). Taken together, these results support a critical role of Tet3 in regulating region-specific DNA demethylation and gene expression in response to global synaptic activity changes.

DISCUSSION

Our results identify Tet3 as a previously unknown global synaptic activity sensor and indicate that even the most fundamental properties

of neurons, such as synaptic transmission and surface GluR1 levels, are dynamically regulated via DNA oxidation and subsequent BER. Active DNA demethylation therefore has a much broader and fundamental role in neurons than previously recognized. Although studies of neuronal DNA damage and repair have traditionally focused on their roles in stress, aging, degenerative neurological disorders and other pathophysiological conditions⁴², our results suggest a previously underappreciated role for DNA repair in normal neuronal physiology and plasticity.

Tet3 has been shown to regulate zygotic paternal DNA reprogramming^{43–45} and embryonic neural development^{46,47}. Recent studies have also shown that Tet1 regulates the expression of some neuronal genes and mouse behavior related to learning and memory^{25,26,48}. Using genetic and pharmacological approaches, we identified physiological functions of Tet3 in neurons and pinpointed the underlying mechanism involving DNA oxidation and active DNA demethylation signaling. Our results suggest a pivotal role for Tet3 in regulating gene expression in response to global synaptic activity changes. Although it is unlikely that all of these genes are directly regulated by Tet3, we identified one bona fide target, *Bdnf*, which is known to regulate synaptic transmission and scaling⁴¹. Notably, activity-induced expression of the immediate early genes *Arc*, *c-Fos*, *Npas4* and *Egr4* required the function of Tet1 (refs. 25,26), but not Tet3 (**Supplementary Fig. 10a**). In addition, Tet1-deficient neurons exhibited hypermethylation at *Arc* and *Npas4* promoters²⁶, which was not the case for Tet3-KD neurons (**Supplementary Fig. 10b**). On the other hand, all of the Tet proteins regulate basal levels of synaptic transmission. Together, these results suggest that Tet family members could have shared, but distinct, roles in neurons.

Homeostatic plasticity allows neurons to sense how active they are and to adjust their properties to maintain stable firing³³. We found that changes in Tet3 expression and DNA demethylation activity mediated both synaptic scaling-up and scaling-down via a classic pathway through *Arc* and GluR1 surface level regulation. Our results are consistent with previous findings that gene transcription is required for TTX-induced synaptic scaling-up⁴⁹ and further describe an unexpected underlying mechanism via DNA oxidation and repair. In a classic view, the major role of epigenetic DNA methylation is to maintain cell identity. Our results extend this view and suggest that, in non-dividing cells, the active DNA demethylation pathway dynamically responds to and processes external stimuli to establish a new cellular state. We provide one example in the nervous system for a critical role of active DNA demethylation in meta-plasticity, a phenomenon in which the history of a neuron's activity determines its current state and its ability to undergo synaptic plasticity⁵⁰.

Beyond advancing our understanding of the functions of Tet3 in regulating neuronal properties and gene expression, our results provide, to the best of our knowledge, the first genetic evidence for a causal role of DNA oxidation and active demethylation in regulating synaptic transmission, which is fundamental to all basic and higher order information processing essential for brain functions. Thus, our findings have broad implications for understanding epigenetic regulation of the nervous system under physiological and pathological conditions.

METHODS

Methods and any associated references are available in the [online version of the paper](#).

Accession codes. The data presented here are available at the Gene Expression Omnibus, under accession code [GSE67245](#).

Note: Any Supplementary Information and Source Data files are available in the online version of the paper.

ACKNOWLEDGMENTS

We thank R. Hugarir, P. Worley, G.C. Turrigiano and L. Chen for suggestions, members of the Ming and Song laboratories for help and critical comments, G.L. Xu for Tet3 antibodies, and L. Liu, Q. Hussaini and Y. Cai for technical support. This work was supported by the US National Institutes of Health (NS047344 to H.S., NS048271 and MH105128 to G.-I.M., NS062691 to G.C. and D.H.G.), a grant from the Simons Foundation (SFARI240011 to H.S.), the Brain and Behavior Research Foundation (H.S., G.-I.M. and Y.S.), Maryland Stem Cell Research Foundation (G.-I.M. and H.S.), and by the Dr. Miriam and Sheldon G. Adelson Medical Research Foundation (G.-I.M., D.H.G. and G.C.). J.S. was supported by a Samsung fellowship.

AUTHOR CONTRIBUTIONS

H.Y. performed electrophysiological analyses. Y.S. performed biochemical and DNA methylation analyses. J.S. and J.U.G. performed bioinformatics analysis. C.Z. and Y.-L.W. generated AAV. F.G., D.H.G. and G.C. performed RNA-seq. G.-I.M. and H.S. designed the project and wrote the manuscript.

COMPETING FINANCIAL INTERESTS

The authors declare no competing financial interests.

Reprints and permissions information is available online at <http://www.nature.com/reprints/index.html>.

1. Tsankova, N., Renthal, W., Kumar, A. & Nestler, E.J. Epigenetic regulation in psychiatric disorders. *Nat. Rev. Neurosci.* **8**, 355–367 (2007).
2. Gräß, J., Kim, D., Dobbin, M.M. & Tsai, L.H. Epigenetic regulation of gene expression in physiological and pathological brain processes. *Physiol. Rev.* **91**, 603–649 (2011).
3. Telese, F., Gamliel, A., Skowronska-Krawczyk, D., Garcia-Bassets, I. & Rosenfeld, M.G. “Seq-ing” insights into the epigenetics of neuronal gene regulation. *Neuron* **77**, 606–623 (2013).
4. Shin, J., Ming, G.L. & Song, H. DNA modifications in the mammalian brain. *Phil. Trans. R. Soc. Lond. B* **369** (2014).
5. Day, J.J., Kennedy, A.J. & Sweatt, J.D. DNA methylation and its implications and accessibility for neuropsychiatric therapeutics. *Annu. Rev. Pharmacol. Toxicol.* **55**, 591–611 (2015).
6. Bird, A. DNA methylation patterns and epigenetic memory. *Genes Dev.* **16**, 6–21 (2002).
7. Law, J.A. & Jacobsen, S.E. Establishing, maintaining and modifying DNA methylation patterns in plants and animals. *Nat. Rev. Genet.* **11**, 204–220 (2010).
8. Martinowich, K. *et al.* DNA methylation-related chromatin remodeling in activity-dependent BDNF gene regulation. *Science* **302**, 890–893 (2003).
9. Miller, C.A. & Sweatt, J.D. Covalent modification of DNA regulates memory formation. *Neuron* **53**, 857–869 (2007).
10. Nelson, E.D., Kavalali, E.T. & Monteggia, L.M. Activity-dependent suppression of miniature neurotransmission through the regulation of DNA methylation. *J. Neurosci.* **28**, 395–406 (2008).
11. Ma, D.K. *et al.* Neuronal activity-induced Gadd45b promotes epigenetic DNA demethylation and adult neurogenesis. *Science* **323**, 1074–1077 (2009).
12. Feng, J. *et al.* Dnmt1 and Dnmt3a maintain DNA methylation and regulate synaptic function in adult forebrain neurons. *Nat. Neurosci.* **13**, 423–430 (2010).
13. Guo, J.U., Su, Y., Zhong, C., Ming, G.L. & Song, H. Hydroxylation of 5-methylcytosine by TET1 promotes active DNA demethylation in the adult brain. *Cell* **145**, 423–434 (2011).
14. Guo, J.U. *et al.* Neuronal activity modifies the DNA methylation landscape in the adult brain. *Nat. Neurosci.* **14**, 1345–1351 (2011).
15. Lister, R. *et al.* Global epigenomic reconfiguration during mammalian brain development. *Science* **341**, 1237905 (2013).
16. Guo, J.U., Su, Y., Zhong, C., Ming, G.L. & Song, H. Emerging roles of TET proteins and 5-hydroxymethylcytosines in active DNA demethylation and beyond. *Cell Cycle* **10**, 2662–2668 (2011).
17. Guo, J.U. *et al.* Genome-wide antagonism between 5-hydroxymethylcytosine and DNA methylation in the adult mouse brain. *Front. Biol. (Beijing)* **9**, 66–74 (2014).
18. Tahiliani, M. *et al.* Conversion of 5-methylcytosine to 5-hydroxymethylcytosine in mammalian DNA by MLL partner TET1. *Science* **324**, 930–935 (2009).
19. Ito, S. *et al.* Role of Tet proteins in 5mC to 5hmC conversion, ES-cell self-renewal and inner cell mass specification. *Nature* **466**, 1129–1133 (2010).
20. Pollen, A.A. *et al.* Low-coverage single-cell mRNA sequencing reveals cellular heterogeneity and activated signaling pathways in developing cerebral cortex. *Nat. Biotechnol.* **32**, 1053–1058 (2014).
21. Pastor, W.A., Aravind, L. & Rao, A. TETonic shift: biological roles of TET proteins in DNA demethylation and transcription. *Nat. Rev. Mol. Cell Biol.* **14**, 341–356 (2013).
22. Kriaucionis, S. & Heintz, N. The nuclear DNA base 5-hydroxymethylcytosine is present in Purkinje neurons and the brain. *Science* **324**, 929–930 (2009).

23. Szulwach, K.E. *et al.* 5-hmC-mediated epigenetic dynamics during postnatal neurodevelopment and aging. *Nat. Neurosci.* **14**, 1607–1616 (2011).
24. Yao, B. *et al.* Genome-wide alteration of 5-hydroxymethylcytosine in a mouse model of fragile X-associated tremor/ataxia syndrome. *Hum. Mol. Genet.* **23**, 1095–1107 (2014).
25. Kaas, G.A. *et al.* TET1 controls CNS 5-methylcytosine hydroxylation, active DNA demethylation, gene transcription and memory formation. *Neuron* **79**, 1086–1093 (2013).
26. Rudenko, A. *et al.* Tet1 is critical for neuronal activity-regulated gene expression and memory extinction. *Neuron* **79**, 1109–1122 (2013).
27. Todarello, G. *et al.* Incomplete penetrance of NRXN1 deletions in families with schizophrenia. *Schizophr. Res.* **155**, 1–7 (2014).
28. Williams, K. *et al.* TET1 and hydroxymethylcytosine in transcription and DNA methylation fidelity. *Nature* **473**, 343–348 (2011).
29. Chen, Q., Chen, Y., Bian, C., Fujiki, R. & Yu, X. TET2 promotes histone O-GlcNAcylation during gene transcription. *Nature* **493**, 561–564 (2013).
30. Ito, S. *et al.* Tet proteins can convert 5-methylcytosine to 5-formylcytosine and 5-carboxylcytosine. *Science* **333**, 1300–1303 (2011).
31. He, Y.F. *et al.* Tet-mediated formation of 5-carboxylcytosine and its excision by TDG in mammalian DNA. *Science* **333**, 1303–1307 (2011).
32. Hajkova, P. *et al.* Genome-wide reprogramming in the mouse germ line entails the base excision repair pathway. *Science* **329**, 78–82 (2010).
33. Turrigiano, G.G. The self-tuning neuron: synaptic scaling of excitatory synapses. *Cell* **135**, 422–435 (2008).
34. Aoto, J., Nam, C.I., Poon, M.M., Ting, P. & Chen, L. Synaptic signaling by all-trans retinoic acid in homeostatic synaptic plasticity. *Neuron* **60**, 308–320 (2008).
35. Lee, H.K. Ca-permeable AMPA receptors in homeostatic synaptic plasticity. *Front. Mol. Neurosci.* **5**, 17 (2012).
36. Koike, M., Iino, M. & Ozawa, S. Blocking effect of 1-naphthyl acetyl spermine on Ca²⁺-permeable AMPA receptors in cultured rat hippocampal neurons. *Neurosci. Res.* **29**, 27–36 (1997).
37. Shepherd, J.D. *et al.* Arc/Arg3.1 mediates homeostatic synaptic scaling of AMPA receptors. *Neuron* **52**, 475–484 (2006).
38. Gao, M. *et al.* A specific requirement of Arc/Arg3.1 for visual experience-induced homeostatic synaptic plasticity in mouse primary visual cortex. *J. Neurosci.* **30**, 7168–7178 (2010).
39. Rial Verde, E.M., Lee-Osbourne, J., Worley, P.F., Malinow, R. & Cline, H.T. Increased expression of the immediate-early gene arc/arg3.1 reduces AMPA receptor-mediated synaptic transmission. *Neuron* **52**, 461–474 (2006).
40. Poo, M.M. Neurotrophins as synaptic modulators. *Nat. Rev. Neurosci.* **2**, 24–32 (2001).
41. Rutherford, L.C., Nelson, S.B. & Turrigiano, G.G. BDNF has opposite effects on the quantal amplitude of pyramidal neuron and interneuron excitatory synapses. *Neuron* **21**, 521–530 (1998).
42. Madabhushi, R., Pan, L. & Tsai, L.H. DNA damage and its links to neurodegeneration. *Neuron* **83**, 266–282 (2014).
43. Gu, T.P. *et al.* The role of Tet3 DNA dioxygenase in epigenetic reprogramming by oocytes. *Nature* **477**, 606–610 (2011).
44. Shen, L. *et al.* Tet3 and DNA replication mediate demethylation of both the maternal and paternal genomes in mouse zygotes. *Cell Stem Cell* **15**, 459–470 (2014).
45. Guo, F. *et al.* Active and passive demethylation of male and female pronuclear DNA in the Mammalian zygote. *Cell Stem Cell* **15**, 447–458 (2014).
46. Xu, Y. *et al.* Tet3 CXXC domain and dioxygenase activity cooperatively regulate key genes for *Xenopus* eye and neural development. *Cell* **151**, 1200–1213 (2012).
47. Hahn, M.A. *et al.* Dynamics of 5-hydroxymethylcytosine and chromatin marks in Mammalian neurogenesis. *Cell Reports* **3**, 291–300 (2013).
48. Zhang, R.R. *et al.* Tet1 regulates adult hippocampal neurogenesis and cognition. *Cell Stem Cell* **13**, 237–245 (2013).
49. Ibata, K., Sun, Q. & Turrigiano, G.G. Rapid synaptic scaling induced by changes in postsynaptic firing. *Neuron* **57**, 819–826 (2008).
50. Abraham, W.C. & Bear, M.F. Metaplasticity: the plasticity of synaptic plasticity. *Trends Neurosci.* **19**, 126–130 (1996).

ONLINE METHODS

Hippocampal neuronal culture, expression constructions, and genetic and pharmacological manipulations. Primary hippocampal neurons were prepared as previously described^{11,51}. Briefly, hippocampi were dissected from E16.5–17.5 mouse embryos (C57BL/6) and dissociated neurons were plated on poly-lysine-coated coverslips in Neurobasal-A medium supplemented with B27 (Invitrogen). AAV gene delivery vectors were constructed by cloning the EF1a-Gene-WPRE cassette⁵² into an AAV backbone by Sall and EcoRV. The shRNA sequences used were listed in **Supplementary Table 1b**. The shRNAs against mouse Tet1, 2, 3 have been previously characterized^{13,19} and we further confirmed their efficacy in primary hippocampal neurons by Q-PCR (**Supplementary Fig. 1c**) and western blot analyses (**Fig. 1b**). Mouse Tet3 cDNA was used for overexpression analysis. AAV-Tet1-CD and AAV-Tet1-mCD has been previously characterized¹³. For AAV-mediated genetic manipulations, engineered AAV coexpressing EYFP or transgenes and shRNA were added into the culture medium at DIV 1 (*day in vitro*). Over 99% cells were infected based on EYFP or transgene expression. Tet3 cDNA was too large for AAV packaging and was directly co-transfected with EYFP cDNA into neurons with Lipofectamine 2000 (Invitrogen) at DIV 4–5. Less than 5% of neurons were transfected based on EYFP expression. For pharmacological treatments, vehicle, ABT (50 μ M) or CRT (50 μ M) was applied for 48 h and RA (1 μ M) was applied for 2 h before analyses. All analyses were performed at DIV 8–9. Synaptic scaling experiments were performed as previously described⁵³. Cultures were treated with 1 μ M TTX or 20 μ M bicuculline for 48 h and then subjected to electrophysiological analyses of mEPSCs, immunocytochemistry or western blot analysis of surface and total GluR1 or GluR2 levels, or dot blot analysis of total 5hmC levels.

Quantitative real-time reverse transcription PCR and mRNA sequencing and analyses. For gene expression analysis, cultured hippocampal neurons were treated with saline, 1 μ M TTX or 20 μ M bicuculline for 4 h in parallel cultures and total RNA was purified using RNeasy Mini Kit (Qiagen). Quantitative real-time PCR was performed with two steps SYBR Green Supermix (ABI). Specific primers (**Supplementary Table 1a**) were used to measure the expression level of target genes with the Ct method as previously described¹³.

RNA-seq analysis was performed as previously described⁵⁴. A total of 17 samples from parallel cultures 4 h after different treatment were used. Sequencing libraries were prepared using Illumina Truseq RNA sample prep kit following manufacturer's protocol. Briefly, total RNA was poly-A tail selected and then heat fragmented. The fragmented RNA was reverse transcribed and the second strand was synthesized to make double-stranded DNA. After end repair and 3' adenylation, adapters for multiplexing were ligated to the end of double-stranded DNA fragments. The ligation products were amplified and purified to generate Illumina compatible libraries. Sequencing was performed with 50 bp paired end multiplexed sequencing by Illumina HiSeq2500. The raw reads were mapped to the mouse genome build mm9 using tophat⁵⁵. The differential expression was called by cuffdiff⁵⁶ with a default FDR of 0.05. Downstream analyses were performed using the Bioconductor EdgeR package⁵⁷ and custom R scripts.

Electrophysiological analysis. Whole-cell patch-clamp recordings ($V_m = -70$ mV) were performed from hippocampal cultures at the DIV 8–9 as previously described⁵⁸. Briefly, micro-pipettes (World Instruments) with 3–7 M Ω resistance were filled with the following internal solution (in mM): potassium gluconate 130, KCl 4, HEPES 10, EGTA 2, ATP 4, GTP 0.3, and phosphocreatine 7 (pH 7.3). The following external solution (in mM) was used: NaCl 140, KCl 3, CaCl₂ 2, MgCl₂ 1.3, HEPES 10, and glucose 10 (pH 7.4). For voltage-clamp recordings of mEPSC, 1 μ M TTX and 20 μ M bicuculline were added to the external solution. Axopatch 200B amplifier (Axon Instruments), Digidata 1322A analog-to-digital converted (Axon Instruments) and pCLAMP 9 software (Axon Instruments) were used for data acquisition. All data was filtered with a low-pass Bessel filter at a frequency of 2 kHz and stored at 5 kHz. pCLAMP 9 and MiniAnalysis software (Synaptosoft) was used for analysis. All experiments were performed in parallel from the same preparation.

Bisulfite sequencing analysis, 5hmC dot blot and ChIP-PCR analyses. Bisulfite sequencing analysis was performed as previously described¹¹. Briefly, bisulfite (Zymo Research)-treated DNA was used as a template for PCR amplification of region of interest with specific primers (**Supplementary Table 1c**). PCR products

were gel-purified and cloned into pCR 2.1 TA (Invitrogen) vector. Individual clones were sequenced and aligned with the reference sequence. A minimum of 15 alleles were examined for each sample and three independent experiments were performed for each condition to obtain mean \pm s.e.m.

Dot blot analysis of 5hmC was performed as previously described¹³. Briefly, genomic DNA samples from different treated groups were adjusted to a concentration of 100 ng μ l⁻¹, heat-denatured at 95 °C for 5 min, and chilled on ice for 1 min. Each sample of 0.1 μ g DNA was applied onto a piece of Hybond-N+ membrane (Amersham), then cross-linked by a UV stratalinker 1800 (Stratagene). Membranes were blocked by 5% dry milk (wt/vol), and then incubated with antibodies (1:10,000 for anti-5hmC, Active motif). Signal was visualized by a HRP-conjugated donkey anti-rabbit IgG antibodies (Santa Cruz) and SuperSignal West Pico Chemiluminescent Substrate (Thermoscientific).

Chromatin immunoprecipitation analysis was performed as previously described¹¹. Briefly, FLAG-Ctrl or FLAG-Tet3 overexpression constructs were electroporated into hippocampal neurons before plating (Amaxa) and cultures were subjected to ChIP at DIV 8 using anti-FLAG antibody (Sigma) following manufacturer's instruction. Specific primers (**Supplementary Table 1d**) were used in PCR to detect the presence of specific DNA binding to Tet3.

Immunocytochemistry, surface biotinylation and western blot analysis. Immunocytochemistry of cultured hippocampal neurons was performed as previously described⁵⁸. Briefly, cells were fixed in 4% paraformaldehyde (wt/vol), subsequently permeabilized with 0.2% Triton X-100 (vol/vol) in phosphate-buffered saline (PBS) for 10 min, then blocked for 1 h in 10% normal donkey serum (vol/vol). Primary antibodies were incubated with neurons overnight at 4 °C, including GFP (Millipore, MAB1083; 1:1,000), Tuj1 (Millipore, MAB5564; 1:2,000), and synapsin I (Millipore, 574777; 1:2,000). Alexa 488-, Alexa 555- or Alexa 647-conjugated secondary antibodies (Molecular Probes; 1:500) to appropriate species were incubated at 22 °C for 2 h. To label surface GluR1, 2.5 μ g of N-terminal GluR1 antibody (Millipore, 07-660; 1:1,000) was added to media and incubated at 10 °C for 30 min. The unbound excess antibody was quickly washed with fresh medium and then fixed and mounted according to the methods described above. All immunocytochemistry experiments were performed from at least three individual batches of cultures for different conditions in parallel. Images were acquired by confocal microscopy (Zeiss 710) using identical settings for parallel cultured and quantified using ImageJ as previously described⁵⁹.

Surface biotinylation was performed as described previously³⁷. Briefly, high-density primary cultured cortical neurons were cooled on ice, washed twice with ice-cold PBS containing 1 mM CaCl₂ and 0.5 mM MgCl₂, and then incubated with 1 mg ml⁻¹ Sulfo-NHS-SS-Biotin (Pierce) for 30 min at 4 °C on a shaker with a gentle speed. The cells were washed three times with ice-cold Quenching solution (100 mM Glycine, pH 7.4) to quench the excess biotin before harvesting the proteins in RIPA buffer. Homogenates were centrifuged at 16,000 g for 20 min at 4 °C. The supernatants were collected, 10% of total volume was saved for total protein analysis. The remaining 90% of the supernatants was incubated with Streptavidin beads (Pierce), and rotated at 4 °C overnight. Precipitates were washed with RIPA buffer three times before heating at 98 °C in SDS-PAGE loading buffer. Surface and total levels of GluRs were analyzed by immunoblotting with N-terminal GluR1 antibody (Millipore, 07-660; 1:1,000) or GluR2 antibodies (Millipore, MAB397; 1:1,000).

Western blot analysis was performed as previously described⁵⁹. Briefly, protein samples were separated by SDS-PAGE and gels were transferred to polyvinylidene difluoride membranes (Millipore) for immunoblot analysis. Blots were incubated in blocking buffer (5% bovine milk (wt/vol) and 0.1% Tween 20 (vol/vol) in PBS, pH 7.4) for 1 h and then in specific primary antibodies overnight at 4 °C, washed in blocking buffer three times for 10 min each, and incubated in corresponding secondary antibodies at 22 °C for 2 h. The following antibodies were used: GluR1-N (Millipore, 07-660; 1:1,000), Tet3 (gift of G.L. Xu⁴³ and Abiocode, M1092-3; 1:3,000) Membranes were stripped and re-blotted with mouse anti-Actin antibodies (Millipore, MAB1501; 1:3,000) as loading control. Western blot images were analyzed by ImageJ. Statistical significance was determined by ANOVA.

Statistics. No statistical methods were used to pre-determine sample sizes but our sample sizes are similar to those generally employed in the field. No randomization and blinding were employed.

A **Supplementary Methods Checklist** is available.

51. Song, H., Stevens, C.F. & Gage, F.H. Astroglia induce neurogenesis from adult neural stem cells. *Nature* **417**, 39–44 (2002).
52. Ge, S. *et al.* GABA regulates synaptic integration of newly generated neurons in the adult brain. *Nature* **439**, 589–593 (2006).
53. Turrigiano, G.G., Leslie, K.R., Desai, N.S., Rutherford, L.C. & Nelson, S.B. Activity-dependent scaling of quantal amplitude in neocortical neurons. *Nature* **391**, 892–896 (1998).
54. Jang, M.H. *et al.* Secreted frizzled-related protein 3 regulates activity-dependent adult hippocampal neurogenesis. *Cell Stem Cell* **12**, 215–223 (2013).
55. Trapnell, C., Pachter, L. & Salzberg, S.L. TopHat: discovering splice junctions with RNA-Seq. *Bioinformatics* **25**, 1105–1111 (2009).
56. Trapnell, C. *et al.* Transcript assembly and quantification by RNA-Seq reveals unannotated transcripts and isoform switching during cell differentiation. *Nat. Biotechnol.* **28**, 511–515 (2010).
57. Robinson, M.D., McCarthy, D.J. & Smyth, G.K. edgeR: a Bioconductor package for differential expression analysis of digital gene expression data. *Bioinformatics* **26**, 139–140 (2010).
58. Song, H.J., Stevens, C.F. & Gage, F.H. Neural stem cells from adult hippocampus develop essential properties of functional CNS neurons. *Nat. Neurosci.* **5**, 438–445 (2002).
59. Kim, J.Y. *et al.* DISC1 regulates new neuron development in the adult brain via modulation of AKT-mTOR signaling through KIAA1212. *Neuron* **63**, 761–773 (2009).